Published in final edited form as:
Chem Commun (Camb). 2011 August 14; 47(30): 8524–8526. doi:10.1039/c1cc12805a.

Kinetic Discrimination in Recognition of DNA Quadruplex Targets by Guanine-Rich Heteroquadruplex-Forming PNA Probes

Subhadeep Roy[a], **Kimberly J. Zanotti**[a], **Connor T. Murphy**[a], **Farial A. Tanious**[b], **W. David Wilson**[b], **Danith H. Ly**[a], and **Bruce A. Armitage**[a,*]

[a]Department of Chemistry and Center for Nucleic Acids Science and Technology, Carnegie Mellon University, 4400 Fifth Avenue, Pittsburgh, PA USA 15213

[b]Department of Chemistry, Georgia State University, Atlanta, GA 30303

Abstract

Guanine-rich peptide nucleic acid probes hybridize to DNA G quadruplex targets with high affinity, forming PNA-DNA heteroquadruplexes. We report a surprising degree of kinetic discrimination for PNA heteroquadruplex formation with a series of DNA targets. The fastest hybridization is observed for targets folded into parallel morphologies.

DNA and RNA guanine quadruplex motifs are the subject of increasing attention due to their suspected roles in regulating transcription, RNA splicing and translation, telomere length and chromosome stability. A variety of strategies are being developed for targeting G-quadruplexes with synthetic compounds, since such reagents would be useful probes of biological function and potential therapeutics. Our labs have adopted a sequence-targeted approach involving peptide nucleic acid (PNA) oligomers that bind with high affinity to quadruplex-forming sequences (QFSs). Rather than using a cytosine-rich PNA to bind to the QFS via Watson-Crick base pairing[1–3], our PNAs are G-rich and bind to both DNA[4,5] and RNA[6,7] QFSs via G-tetrad formation, yielding heteroquadruplexes with low nanomolar dissociation constants. The PNAs typically consist of two G_n tracts, allowing them to bind to a quadruplex target, which has at least four G_n tracts, in a 2:1 stoichiometry.[5,7] Our group and others have shown that a variety of backbone modifications[8, 9] or the addition of a stacking ligand[10] provide additional opportunities for enhancing the quadruplex binding affinity and/or selectivity of G-rich PNAs.

Based on our earlier results, we were motivated to investigate hybridization of the PNA to a variety of other DNA quadruplexes in order to define the scope of possible targets that could be recognized by this binding mode. Table S1 lists the sequences that were studied; **Myc19** was the subject of our earlier reports and was included for comparison with the new targets. The **VEGF**, **cKIT22** and **Bcl2** quadruplexes are derived from oncogene promoter sequences, while **hTelo22** is based on the human telomeric repeat sequence $(GGGTTA)_n$. All five of these quadruplexes consist of three stacked G tetrads, but exhibit considerable variation in the morphology, as determined by multidimensional NMR spectroscopy and/or circular dichroism spectroscopy.[11–16]

Fax: 412-268-1061; Tel: 412-268-4196; army@cmu.edu.

Electronic Supplementary Information (ESI) available: PNA synthesis details and supporting SPR and CD data.

We used our previously reported quadruplex-forming PNA probe **P_{myc}** (H-GGGAGGGG-$LysNH_2$) for our initial experiments. Figure 1 shows the results of surface plasmon resonance (SPR) experiments in which the various DNA targets were immobilized on a streptavidin-coated carboxymethyl-dextran chip while the PNA was allowed to flow over the surface of the chip. A surprising degree of kinetic discrimination is observed in the SPR sensorgrams. The fastest hybridization occurs for the **Myc19** and **VEGF** quadruplexes, with intermediate on-rates observed for **cKit22** and **Bcl2**. By far the slowest hybridization is observed for the telomeric quadruplex **hTelo22**, although we note that the relatively small amount of PNA that binds to this target is also slow to dissociate.

Based on the SPR results, we selected the most disparate targets, **Myc19** and **hTelo22** for further study. To determine whether the kinetic discrimination between these two targets was specific to **P_{myc}**, we performed SPR experiments with two other PNAs, **P_{telo}** (H-GGGTTAGGG-$LysNH_2$) and **P_{eg2}** (H-GGG-eg_2-GGG-$LysNH_2$, where *eg* corresponds to an abasic spacer residue[9]). As shown in supporting information, both of these PNAs bound much faster to **Myc19** than to **hTelo22** (Fig. S1), indicating that the kinetic advantage in targeting **Myc19** is due to an inherent property of the DNA quadruplex, not the PNA probe.

UV melting curves for the two DNA quadruplexes alone and in the presence of **P_{myc}** are shown in Figure 2. Two equivalents of the PNA were used in both cases based on the expected stoichiometries of the heteroquadruplexes[5,9] and a low KCl concentration (1 mM) was used to allow observation of all melting transitions. The **hTelo22** homoquadruplex melts at significantly lower temperature than the **Myc19** homoquadruplex. Melting of the corresponding heteroquadruplexes occurs at much higher temperatures, with ΔT_m = 24.9 °C and 17.4 °C for **hTelo22** and **Myc19**, respectively. The heteroquadruplexes were destabilized by > 10 °C when KCl was replaced by LiCl, as expected for structures stabilized by G-tetrads (data not shown).

Circular dichroism spectroscopy provided additional insight into the differences in hybridization of **P_{myc}** to the two DNA quadruplexes. As shown in Figure 3, **Myc19** exhibits positive and negative extrema at 260 nm and 240 nm, respectively, and these features are retained upon PNA hybridization, consistent with our earlier reports. **hTelo22** alone exhibits a peak at 295 nm with a weaker shoulder at 260 nm, as expected for the “hybrid” folded structure of this quadruplex, which contains a mixture of parallel and antiparallel strand orientations.[16] When the PNA is present, the 295 nm peak is maintained, but the 260 nm peak grows to be nearly equal in intensity. Thus, the structure of the heteroquadruplex appears to contain a mixture of parallel and antiparallel features, although there is perhaps a shift in favor of parallel strand orientations.

The results shown in Figure 1 indicate that heteroquadruplex formation by **P_{myc}** occurs fastest for the purely parallel targets, **Myc19** and **VEGF**, while the noncanonical parallel structure of **cKit22**, in which one of the G_3 tracts is formed by a noncontiguous set of guanines, and the two hybrid quadruplexes, are less easily invaded by the PNA. Based on these observations, we decided to investigate one additional quadruplex target, **rHT3** (Table S1). This chimeric molecule has the same sequence as **hTelo22** but features two G_3 tracts based on ribonucleotides while the remaining G_3 tracts (and loops) retain deoxyribonucleotides. Shafer previously demonstrated that **rHT3** exhibits a CD spectrum reminiscent of **Myc19**, suggesting that **rHT3** adopts a parallel conformation rather than the hybrid structure of **hTelo22**.[17] The parallel CD spectrum of **rHT3** is preserved in the presence of **P_{myc}** (Figure S2). As shown in Figure 4, **P_{myc}** hybridizes much faster to **rHT3** than to **hTelo22**, consistent with a kinetic preference for hybridizing parallel quadruplex structures.

Our previous experiments revealed that **P_{myc}** binds to **Myc19** with a 2:1 stoichiometry and an average K_d = 5.0 nM, as determined by a competition SPR method that allows analysis of heteroquadruplex formation in solution.[5] We used the same method to analyze binding of **P_{myc}** to **hTelo22** and **rHT3** and again found that the data were well fit by a 2:1 equivalent site binding model, with an average K_d = 12.5 nM and 0.7 nM, respectively (Figures S3–S6). Thus, the much slower association rate for **hTelo22** relative to **Myc19** is almost completely offset by slower dissociation kinetics, resulting in K_d values that differ by only a factor of 2.5. Meanwhile, the significantly lower K_d for the chimeric quadruplex **rHT3** represents the first sub-nanomolar K_d we have determined for PNA-containing heteroquadruplexes.

Further experiments are required to understand the wide range of hybridization kinetics shown in Figures 1 and 4. While our strategy exhibits some level of sequence selectivity, which can be tuned by varying the PNA backbone and loop composition,[9] the kinetic data suggest possible structure selectivity as well. An interesting distinction within the set of five DNA quadruplexes targeted in Figure 1 concerns the deoxyguanosine (dG) nucleoside conformations: for **Myc19** and **VEGF**, all of the dGs adopt the *anti* conformation, whereas the **hTelo22** and **cKit22** quadruplexes feature a mixture of *syn* and *anti* conformations. Whether this difference contributes to the kinetic selectivity remains to be seen, but we can speculate on how this might play a role. The CD data indicate that PNA-DNA heteroquadruplexes favor *anti* dG conformations, since the spectrum of **Myc19** is unchanged by the PNA, while the spectrum of **hTelo22** exhibits an enhanced signal at 260 nm. If there is indeed a preference for the *anti* conformation, then this could account for the slower PNA hybridization to the hybrid and noncanonical parallel targets. As shown in Scheme 1, PNA invasion of a quadruplex in which all of the dGs are *anti* requires severing only 4 of the 8 hydrogen bonds per G tetrad, since this allows the quadruplex to open (like a book), creating two binding surfaces for the PNAs. In contrast, if a dG is in a *syn* conformation, then severing 6 hydrogen bonds might be needed to allow the guanine rotation needed to convert from *syn* to *anti* prior to PNA hybridization. This model is supported by Shafer's findings that ribo-substitutions favor *anti* conformations,[17, 18] as in the case of **rHT3**, which exhibited much faster PNA hybridization kinetics than the isosequential hybrid quadruplex **hTelo22**.

Conclusions

DNA and RNA recognition by heteroquadruplex formation offers distinctive opportunities for recognition of G-rich sequence and structural motifs. While thermodynamic selectivity has been tuned through variation of the PNA structure, this is the first example of kinetic discrimination among different quadruplex targets. Of course, the preferences observed in these experiments might not carry over to cellular contexts, where protein binding and alternative secondary/tertiary structures could interfere with PNA hybridization. Nevertheless, the results do indicate that parallel structures offer an inherently more accessible target. Recent work indicates that sequences capable of forming parallel quadruplexes are prevalent in the genome[19,20] and could provide a rich array of binding sites for a quadruplex-forming PNA.

Supplementary Material

Refer to Web version on PubMed Central for supplementary material.

Acknowledgments

The authors thank the United States National Institutes of Health for support of this research (R01 GM58547 to BAA and R01 AI064200 to WDW). KJZ acknowledges support from a U.S. DoD Air Force Office of Scientific Research NDSEG Fellowship 32 CFR 168a. SPR instrumentation was purchased with support from NSF MRI award 0821296.

Notes and references

1. Green JJ, Ying L, Klenerman D, Balasubramanian S. J Am Chem Soc. 2003; 125:3763–3767. [PubMed: 12656607]
2. Datta B, Armitage BA. J Am Chem Soc. 2001; 123:9612–9619. [PubMed: 11572682]
3. Amato J, Oliviero G, De Pauw E, Gabelica V. Biopolymers. 2009; 91:244–255. [PubMed: 19065573]
4. Datta B, Schmitt C, Armitage BA. J Am Chem Soc. 2003; 125:4111–4118. [PubMed: 12670232]
5. Roy S, Tanious F, Wilson WD, Ly DH, Armitage BA. Biochemistry. 2007; 46:10433–10443. [PubMed: 17718513]
6. Marin VL, Armitage BA. J Am Chem Soc. 2005; 127:8032–8033. [PubMed: 15926825]
7. Marin VL, Armitage BA. Biochemistry. 2006; 45:1745–1754. [PubMed: 16460021]
8. Englund EA, Xu Q, Witschi MA, Appella DH. J Am Chem Soc. 2006; 128:16456–16457. [PubMed: 17177367]
9. Lusvarghi S, Murphy CT, Roy S, Tanious FA, Sacui I, Wilson WD, Ly DH, Armitage BA. J Am Chem Soc. 2009; 131:18415–18424. [PubMed: 19947597]
10. Paul A, Sengupta P, Krishnan Y, Ladame S. Chem Eur J. 2008; 14:8682–8689.
11. Ambrus A, Chen D, Dai J, Jones RA, Yang D. Biochemistry. 2005; 44:2048–2058. [PubMed: 15697230]
12. Phan AT, Modi YS, Patel DJ. J Am Chem Soc. 2004; 126:8710–8716. [PubMed: 15250723]
13. Sun D, Liu WJ, Guo K, Rusche JJ, Ebbinghaus S, Gokhale V, Hurley LH. Mol Cancer Ther. 2008; 7:880–889. [PubMed: 18413801]
14. Phan AT, Kuryavi V, Burge S, Neidle S, Patel DJ. J Am Chem Soc. 2007; 129:4386–4392. [PubMed: 17362008]
15. Dai J, Dexheimer TS, Chen D, Carver M, Ambrus A, Jones RA, Yang D. J Am Chem Soc. 2006; 128:1096–1098. [PubMed: 16433524]
16. Ambrus A, Chen D, Dai J, Bialis T, Jones RA, Yang D. Nucleic Acids Res. 2006; 34:2723–2735. [PubMed: 16714449]
17. Qi J, Shafer RH. Biochemistry. 2007; 46:7599–7606. [PubMed: 17539606]
18. Tang CF, Shafer RH. J Am Chem Soc. 2006; 128:5966–5973. [PubMed: 16637665]
19. Huppert J, Balasubramanian S. Nucleic Acids Res. 2008; 35:406–413. [PubMed: 17169996]
20. Bugaut A, Balasubramanian S. Biochemistry. 2008; 47:689–697. [PubMed: 18092816]

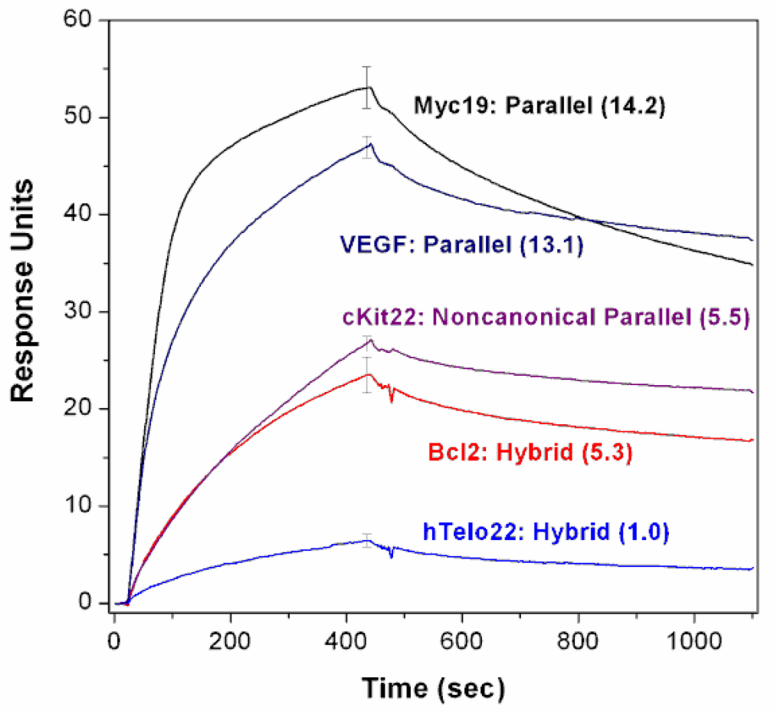

Fig. 1.

SPR sensorgrams for hybridization of $\mathbf{P_{myc}}$ (10 nM) to immobilized DNA quadruplex targets. Vertical error bars reflect standard deviations for three separate experiments. Numbers in parentheses indicate initial rates of association, relative to **hTelo22**.

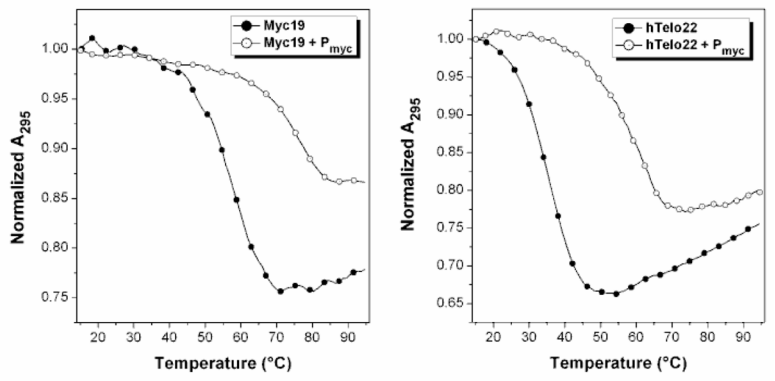

Fig. 2.

UV melting curves recorded for 1.0 μM **Myc19** (left) and **hTelo22** (right) with and without 2 equiv $\mathbf{P_{myc}}$. Data were normalized to the A_{295} value at 15 °C.

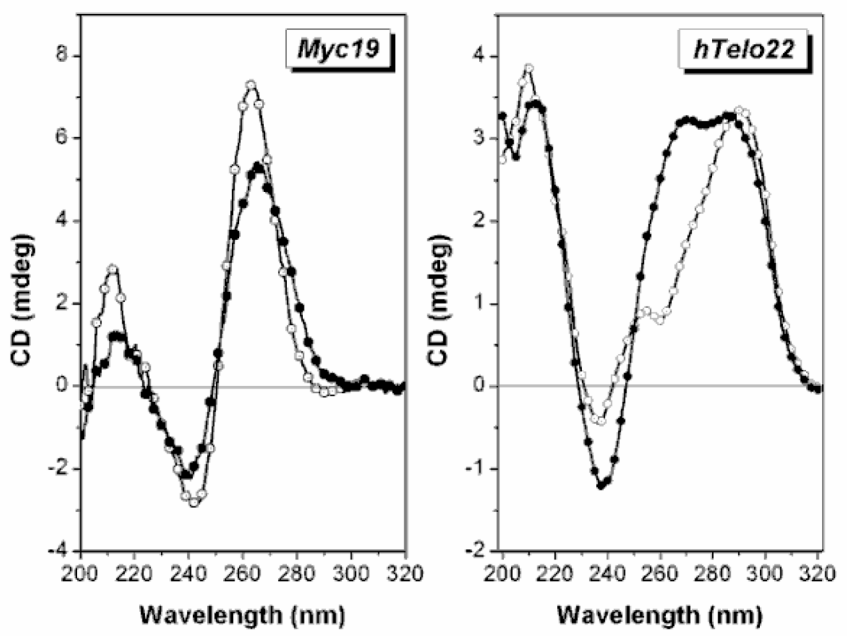

Fig. 3.

Circular dichroism spectra recorded for 1.0 μM **Myc19** (left) and **hTelo22** (right) with and without 2 equiv $\mathbf{P_{myc}}$. Samples contained 100 mM KCl. Open circles: DNA alone; filled circles: DNA + PNA.

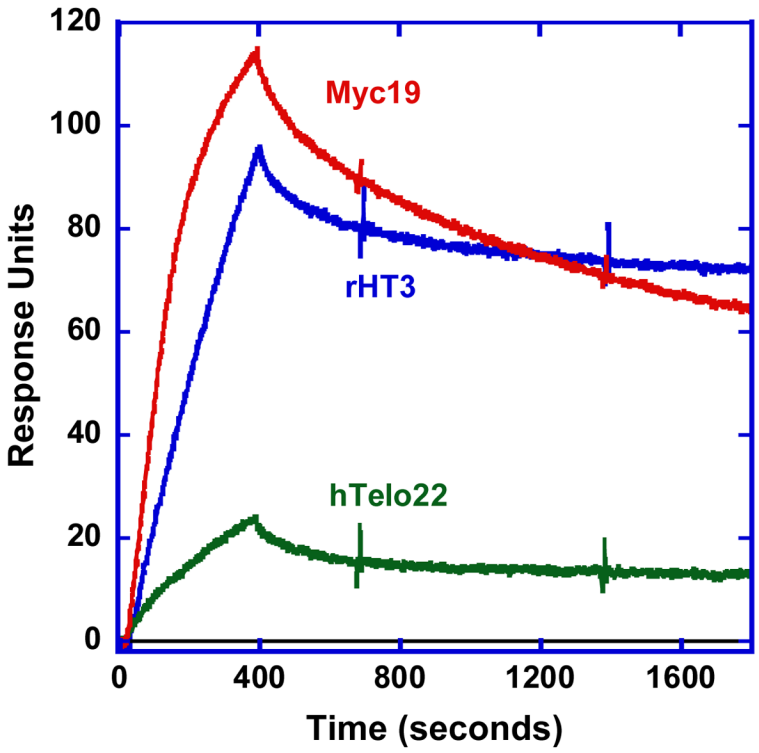

Fig. 4.
SPR sensorgrams for hybridization of $\mathbf{P_{myc}}$ (40 nM) to immobilized **Myc19**, **rHT3** and **hTelo22** quadruplexes.

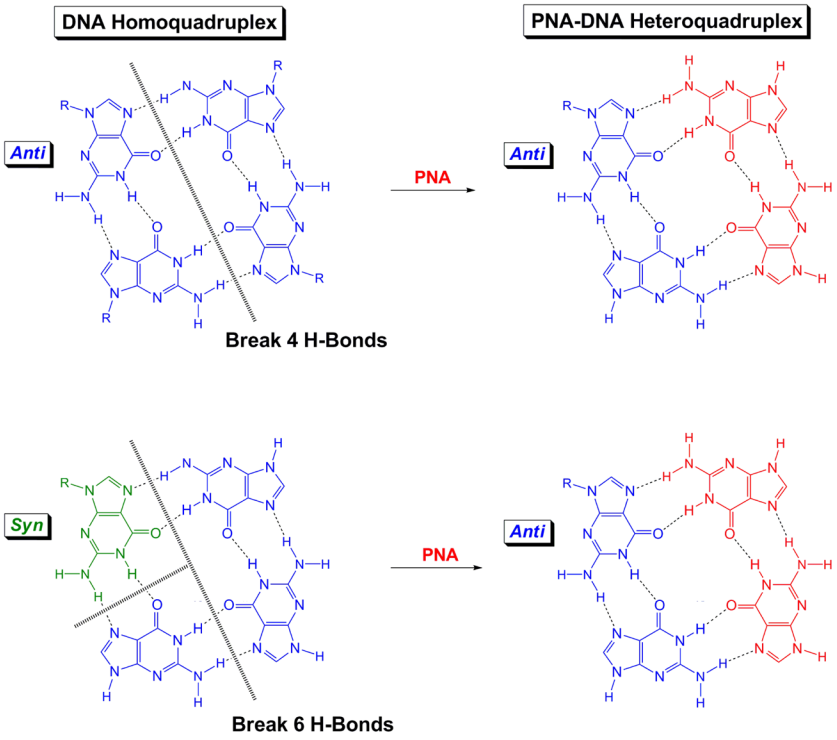

Scheme 1.
Comparison of PNA-DNA heteroquadruplex formation involving targets containing all *anti* or *anti/syn* nucleoside conformations